Crystallization of a Layered Silicate Clay as Monitored by Small-Angle X-ray Scattering and NMR

K. A. Carrado,* L. Xu, D. M. Gregory,† K. Song,‡ S. Seifert, and R. E. Botto

Chemistry Division, Argonne National Laboratory, 9700 South Cass Avenue, Argonne, Illinois 60439

Received May 3, 2000. Revised Manuscript Received July 18, 2000

The 48-h hydrothermal crystallization of a magnesium silicate clay called hectorite has been investigated in detail. Tetraethylammonium (TEA) ions are used to aid crystallization and become incorporated as the exchange cations within the interlayers. Data from small-angle X-ray scattering (SAXS) using aliquots ex situ are consistent with results obtained previously by X-ray powder diffraction (XRD), thermal gravimetric analysis (TGA), atomic force microscopy (AFM), and IR. All these techniques see clay crystallites beginning to form within the first few hours of reaction. ^{29}Si NMR displays a visible clay silicate peak after just 1 h. Solid-state ^{13}C NMR shows evidence of TEA−clay formation in as little as 30 min and also that 80% of the final TEA loading is accomplished in the first 10−12 h. Up to 36 h more is needed to incorporate the remaining 20% of TEA, indicating that a slower event is dominating at the later stages of crystallization. Data from ^{13}C NMR and SAXS are compared to and are consistent with data from earlier AFM experiments. All present a scenario where initial nucleation and crystallization end after about 14 h, after which this occurs to a lesser extent and primarily agglomeration of particles is taking place. The SAXS data show this in progressively increasing power law values, indicating more "open" structures that condense into more dense structures with time. In addition, the first in situ study of clay crystallization of any kind was performed by in situ SAXS. A possible clay crystallization mechanism is proposed.

Introduction

The mechanism of formation of clays has been reviewed recently and is of interest because synthetic layered silicates are used as heterogeneous catalyst supports and in various other technological applications.[1,2] A full understanding of the mechanism would help direct tailored synthetic processes. The complete crystallization of a 2:1 magnesium silicate smectite clay called hectorite takes just 48 h at 100 °C when quaternary ammonium compounds are used to provide the exchangeable cation.[3] This formation has been monitored by several ex situ techniques wherein samples are removed and isolated after progressive crystallization times.[3−5] These techniques reveal that significant clay growth occurs within the first few hours of the hydrothermal reaction of the aqueous mixture containing silica, magnesium hydroxide (brucite), lithium fluoride, and a quaternary ammonium salt. Evidence of clay peaks in X-ray powder diffraction (XRD) occurs after just 4 h and brucite is no longer observable by XRD after 14 h.[4] Observable changes by thermal analysis and IR methods occur at about 4−6 h as well.[4] Studies using atomic force microscopy (AFM) reveal that Ostwald ripening is apparent in this system in certain time frames.[5] We have now exploited both small-angle X-ray scattering (SAXS) and solid-state NMR techniques to access different size regimes, length scales, and time frames, to add information to the overall scenario of a clay crystallization mechanism.

SAXS techniques have been used with some regularity over many years in clay science to determine dispersion parameters such as particle size and thickness in solvated systems.[6] They have also been applied to clay studies concerning microstructure,[7] adsorption of organics,[8] fractal dimensions,[9] metal loading,[10] and aggregation.[11] Solid-state NMR techniques have been

* To whom correspondence should be addressed. Phone: (630)252-7968. Fax: (630)252-9288. E-mail: kcarrado@anl.gov.

† Current address: Quantum Magnetics, 7740 Kenamar Court, San Diego, CA 92121.

‡ Current address: Novellus Systems, Inc., 4041 N. First Street, San Jose, CA 95134.

(1) Kloprogge, J. T. *J. Porous Mater.* **1998**, *5*, 5.

(2) Kloprogge, J. T.; Komarneni, S.; Amonette, J. E. *Clays Clay Miner.* **1999**, *47*, 529.

(3) Carrado, K. A.; Thiyagarajan, P.; Winans, R. E.; Botto, R. E. *Inorg. Chem.* **1991**, *30*, 794.

(4) Carrado, K. A.; Thiyagarajan, P.; Song, K. *Clay Miner.* **1997**, *32*, 29.

(5) Carrado, K. A.; Zajac, G. W.; Song, K.; Brenner, J. R. *Langmuir* **1997**, *13*, 2895.

(6) (a) Saunders, J. M.; Goodwin, J. W.; Richardson, R. M.; Vincent, B. *J. Phys. Chem. B* **1999**, *103*, 9211. (b) Faisandier, K.; Pons, C. H.; Tchoubar, D.; Thomas, F. *Clays Clay Miner.* **1998**, *46*, 636. (c) Pignon, F.; Magnin, A.; Piau, J.-M.; Cabane, B.; Lindner, P.; Diat, O. *Phys. Rev. E* **1997**, *56*, 3281. (d) Morvan, M.; Espinat, D.; Lambard, J.; Zemb, T. *Colloids Surf. A* **1994**, *82*, 193. (e) Hight, R.; Higdon, W. T.; Darley, H. C. H.; Schmidt, P. W. *J. Chem. Phys.* **1962**, *37*, 502. (f) Hight, R.; Higdon, W. T.; Schmidt, P. W. *J. Chem. Phys.* **1960**, *33*, 1656.

(7) Ben Rhaiem, H.; Ben Haj Amara, A.; Ben Brahim, J.; Pons, C. H. *Mater. Sci. Forum* **1998**, *278−281*, 868.

(8) Pernyeszi, T.; Patzko, A.; Berkesi, O.; Dekany, I. *Colloids Surf. A* **1998**, *137*, 373.

(9) Malekani, K.; Rice, J. A.; Lin, J.-S. *Clays Clay Miner.* **1996**, *44*, 677.

(10) Kiraly, Z.; Dekany, I.; Mastalir, A.; Bartok, M. *J. Catal.* **1996**, *161*, 401.

10.1021/cm000366a CCC: $19.00
Published on Web 09/19/2000

widely applied to aspects of clay chemistry[12] such as lattice structure (^{29}Si, ^{27}Al),[13] interlayer cations (^{23}Na, ^{113}Cd, ^{133}Cs),[14] and organic adsorption (^{1}H, ^{13}C, ^{31}P).[15] The power of the NMR technique for studying reactions involving clays is demonstrated by a report using ^{13}C CP MAS of intercalated molecules, where the progress of the polymerization of acrylamide to polyacrylamide on kaolinite was monitored by the disappearance of the C═C bonds.[16] There has been one previous report using ^{29}Si MAS NMR to examine the gel synthesis of magnesium silicates,[17] although they were not clays. The use of NMR for analogous structural determinations in zeolites has recently been reviewed,[18] along with applicable studies to follow zeolite formation.[19] There have even been a few reports utilizing SAXS to analyze zeolite precursors.[20] To the best of our knowledge, this is the first time that the combination of SAXS and solid-state NMR techniques has been applied to monitor any type of clay crystallization process.

Experimental Section

Materials. The typical method for in situ hydrothermal crystallization of organo-hectorite clays is to create a 2 wt % gel of silica sol, magnesium hydroxide sol, lithium fluoride, and organic in water and to reflux for 2 days. Complete details can be found elsewhere.[4,5,21] Reagents were purchased from Aldrich. The organic of choice for these crystallization studies is tetraethylammonium chloride (TEA). Precursor clay gels are of the composition

$$0.32\text{TEA},\ 1.0\text{LiF},\ 5.3\text{Mg(OH)}_2,\ 8\text{SiO}_2,\ n\text{H}_2\text{O}$$

to correlate with the ideal hectorite composition[22] of $Ex_{0.66}[Li_{0.66}Mg_{5.34}Si_8O_{20}(OH,F)_4]$, where Ex is exchangeable cation (Ex is Li, TEA from this gel). Note that Li(I) is an isomorphous substituion for Mg(II) at about 1:9.6. This gives rise to the net negative charge on the basal oxygen plane that is compensated for with the exchangeable TEA cations. As in all smectite clays, two tetrahedral silicate layers sandwich a central metal oxide (in this case magnesium) octahedral layer.

A typical reaction begins by dissolving 0.72 mmol of TEA in water and adding 4.8 mmol of LiF with stirring. Separately, 24 mmol of $MgCl_2 \cdot 6H_2O$ is dissolved in water and mixed with 32 mL of 2 N NH_4OH to crystallize fresh $Mg(OH)_2$. Prior to use, this brucite source must be washed several times with water to remove excess ions. It is then added wet to the organic−LiF solution. This slurry is stirred for about 15 min before addition of 0.036 mol of silica sol (Ludox HS-30, Na^+-stabilized, 30 wt %, particle diameter 12 nm). This mixture is refluxed for up to 48 h and then centrifuged and the products are washed and air-dried. Small aliquots for ex situ time-resolved studies are removed at various times during the crystallization. Powder samples are isolated after centrifuging, washing, and drying. Wet gels are saved as is without further washing.

SAXS Analysis. The SAXS instrument was constructed at Argonne National Laboratory (ANL) and used on the Basic Energy Sciences Synchrotron Radiation Center undulator beam line ID-12 at the Advanced Photon Source.[23,24] For the ex situ gel studies, wet aliquots were concentrated via centrifugation and transferred to 1.5-mm quartz capillary tubes obtained from the Charles Supper Co., Natick, MA. The SAXS data were collected in 5-min exposures (scans). Controls of pure silica and brucite sols (diluted to appropriate concentrations) were also run in capillaries. For the in situ study, a small portion of unreacted clay gel was transferred to a 1.5-mm quartz capillary tube and sealed (the gel was first preconcentrated by 75%). This capillary was placed in a home-built furnace assembly such that the gel was directly in the beam path. The temperature was computer-controlled; scanning began at 70 °C, which took only 3−4 min to reach. Within 5 min the temperature had reached 100 °C and held within ±1 °C for the duration of the run. SAXS data were collected in 2-min scans separated by 5 μs for the first 2 h and then as 10-min scans for the remaining 10 h. Monochromatic X-rays at 10.0 keV were scattered off the sample and collected on a 19 × 19 cm^2 position-sensitive two-dimensional gas wire detector. The scattered intensity has been corrected for absorption, scattering from a blank capillary containing only water (or scattering from blank scotch tape for the powder studies), and instrument background.

The differential scattering cross section can be expressed as a function of the scattering vector Q, which is defined as $Q = (4\pi/\lambda) \sin\theta$, where λ is the wavelength of the X-rays and θ is the scattering half angle. The value of Q is proportional to the inverse of the length scale (Å^{-1}). The instrument was operated at a sample-to-detector distance of 67.0 cm to obtain data at $0.04 < Q < 0.7$ Å^{-1} (so-called "high-Q") and at 389 cm for the range $0.007 < Q < 0.16$ Å^{-1} (so-called "low-Q"). Whereas Kapton windows were used for the lower Q range data, Mylar windows had to be utilized for the higher Q range because it does not have diffraction peaks in this region.

For ex situ powder studies, the same powders as those used for the NMR analyses were sprinkled onto and sealed in scotch tape "cells". A newer nine-element mosaic CCD detector (15 × 15 cm^2) with a maximum of 3000 × 3000 pixel resolution was utilized for these samples. This detector can better accommodate the high scattering intensities of these clay samples and required only 0.1-s exposure times. Other parameters were enhanced as well: an evacuated sample chamber was utilized and the effective Q-range was 0.002−0.07 Å^{-1} (the sample-to-detector distance was 296 cm in this configuration). Error bars are not shown in any of the figures only for the sake of clarity; they are of equal or lesser size than the data points except at very high-Q values.

(11) Dwiggins, C. W. *J. Appl. Crystallogr.* **1982**, *15*, 564.
(12) Goodman, B. A.; Chudek, J. A. In *Clay Mineralogy: Spectroscopic and Chemical Determinative Methods*; Wilson, M. J., Ed.; Chapman & Hall: London, 1994; Chapter 4.
(13) (a) Sanz, J.; Robert, J.-L. *Phys. Chem. Miner.* **1992**, *19*, 39. (b) Hayashi, S.; Ueda, T.; Hayamizu, K.; Akiba, E. *J. Phys. Chem.* **1992**, *96*, 10922. (c) Komarneni, S.; Fyfe, C. A.; Kennedy, G. J.; Strobl, H. *J. Am. Ceram. Soc.* **1986**, *69*, C45. (d) Weiss, C. A.; Altaner, S. P.; Kirkpatrick, R. J. *Am. Miner.* **1987**, *72*, 935. (e) Alma, N. C. M.; Hays, G. R.; Samoson, A. V.; Lippmaa, E. T. *Anal. Chem.* **1984**, *56*, 729.
(14) (a) Kloprogge, J. T.; Jansen, J. B. H.; Schuiling, R. D.; Geus, J. W. *Clays Clay Miner.* **1992**, *5*, 561. (b) Tinet, D.; Faugere, A. M.; Prost, R. *J. Phys. Chem.* **1991**, *95*, 8804. (c) Weiss, C. A.; Kirkpatrick, R. J.; Altaner, S. P. *Am. Miner.* **1990**, *75*, 970. (d) Laperche, V.; Lambert, J. F.; Prost, R.; Fripiat, J. J. *J. Phys. Chem.* **1990**, *94*, 8821.
(15) (a) Hayashi, S.; Akiba, E. *Chem. Phys. Lett.* **1994**, *226*, 495. (b) Carrado, K. A.; Hayatsu, R.; Botto, R. E.; Winans, R. E. *Clays Clay Miner.* **1990**, *38*, 250. (c) Kumar, K. R.; Choudary, B. M. *J. Mol. Catal.* **1987**, *40*, 327. (d) Fyfe, C. A.; Thomas, J. M.; Lyerla, J. R. *Angew. Chem., Int. Ed. Engl.* **1981**, *20*, 96.
(16) Sugahara, Y.; Satokawa, A.; Kuroda, K.; Kato, C. *Clays Clay Miner.* **1990**, *38*, 137.
(17) Hartman, J. S.; Millard, R. L. *Phys. Chem. Miner.* **1990**, *17*, 1.
(18) Karge, H. G.; Hunger, M.; Beyer, H. K. In *Catalysis and Zeolites*; Weitkamp, J., Puppe, L., Eds.; Springer: Berlin, 1999; p 198.
(19) (a) Shi, J.; Anderson, M. W.; Carr, S. W. *Chem. Mater.* **1996**, *8*, 369. (b) Weigel, S. J.; Gabriel, J.-C.; Guttierez Puebla, E.; Monge Bravo, A.; Henson, N. J.; Bull, L. M.; Cheetham, A. K. *J. Am. Chem. Soc.* **1996**, *118*, 2427. (c) Gittleman, C. S.; Watanabe, K.; Bell, A. T.; Radke, C. J. *Microporous Mater.* **1996**, *6*, 131. (d) Burkett, S. L.; Davis, M. E. *Chem. Mater.* **1995**, *7*, 920.
(20) (a) Dougherty, J.; Iton, L. E.; White, J. W. *Zeolites* **1995**, *15*, 640. (b) Regev, O.; Cohen, Y.; Kehat, E.; Talmon, Y. *Zeolites* **1994**, *14*, 314. (c) Beelen, T. P. M.; Dokter, W. H.; van Garderen, H. F.; van Santen, R. A.; Browne, M. T.; Morrison, G. R. *Mater. Res. Soc. Symp. Proc.* **1992**, *271*, 263.
(21) Carrado, K. A. *Appl. Clay Sci.* **2000**, *17*, 1.
(22) Grim, R. E. *Clay Mineralogy*; McGraw-Hill: New York, 1968; p 68.
(23) Winans, R. E.; Seifert, S.; Thiyagarajan, P. *Am. Chem. Soc. Div. Fuel Chem. Prepr.* **1999**, *44*, 576−580.
(24) For a full description of the instrument see http://www.bessrc.aps.anl.

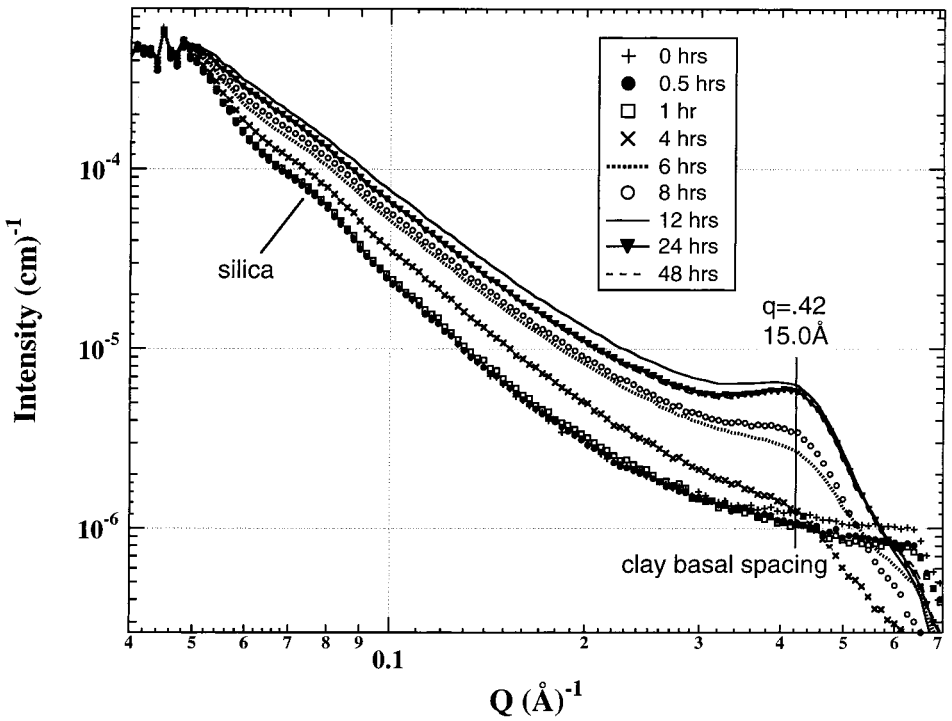

Figure 1. SAXS in the higher-*Q* data regime of ex situ synthetic TEA−hectorite gel aliquots taken at various times as indicated in the legend.

NMR Analysis. NMR data were acquired on a Bruker Advance DSX-200 spectrometer operating at a ^{13}C Larmor frequency of 50.3 MHz. A Bruker 7-mm MAS probe and a simple 90°- pulse-acquire experiment was used for all experiments. Sample spinning was maintained at 4000 ± 2 Hz. Data were acquired in the presence of proton decoupling with proton power set to 80 kHz. The 90°-pulse times were 6.5 and 7.0 μs for ^{13}C and ^{29}Si, respectively. Recycle delays were 3 and 200 s for ^{13}C and ^{29}Si experiments, respectively. The number of transients recorded were 2400 and 128 for ^{13}C and ^{29}Si spectra, respectively. All spectra were referenced to TMS. Hexamethylbenzene was used as a secondary reference for ^{13}C spectra, and TKS was used as a secondary reference for ^{29}Si spectra.[25] All samples were packed to the same level in the rotor; however, because of variations in density, the sample weight varied from 114 to 153 mg. Thus, the data points in Figure 9 were normalized by weight. No attempt was made to normalize the spectra in the stacked plots (Figures 7 and 8).

Results and Discussion

SAXS Studies—High-*Q* Regime. Results from the high-*Q* SAXS using aliquots ex situ show, first, that data for both isolated dried powders and the wet gels are consistent with each other. This has implications for SAXS sample preparation in that for convenience either form (wet or dry) can be used. Figure 1 shows the data from the gels. Scattering from the starting material silica sol (seen at about 0.08 Å^{-1}) gradually disappears as the clay crystallizes and scatters in the basal spacing region (0.4 Å^{-1}, 15 Å). This phenomenon is visibly evident at about 6 h. High background levels in the highest-*Q* region that are probably due to brucite scattering (as seen in the control sample that was measured) disappear sooner, between 1 and 4 h. These data are consistent with ex situ XRD, TGA, and IR data in that all these techniques see clay crystallites beginning to form after about 4 h of reaction.

In addition, the first in situ study of clay crystallization of any kind was performed by in situ SAXS. Data were collected every 2 min for 2 h and then every 10 min for 10 h. These data are shown in Figure 2 with only a few representative curves displayed. Results are consistent with the ex situ data. There is background scatter in the high-*Q* basal spacing region well past the 4-h point at which it disappears for ex situ samples. It is suspected that this is due to the overall weak intensity of the signal due to a low concentration of clay in the beam (note the low intensity at $Q = 0.04$ Å^{-1}, especially as time progresses).

SAXS Studies—Low-*Q* Regime. In contrast to the high-*Q* data, the differences between using gel and powder samples are striking in this range. For gel samples the background silica scattering dominates the signal at all clay crystallization times. This obscures clear observation of clay scattering and therefore the curves are not shown. A Guinier analysis (log I vs Q^2) of the control sample of silica sol alone yields a radius of gyration (R_g) of 75 Å, which is consistent with values from the supplier. This feature persists in all curves out to even the 48-h crystallized product. To most efficiently use data in this range, the gels need to be thoroughly washed prior to analysis. We further conclude that doing an in situ study in this region would be counterproductive because of the required presence of silica.

The ex situ powder samples of Figures 3−5 are more informative, especially at the very early crystallization times, in the low-*Q* regime. There are two large mid-*Q* range humps in the scattering curve of the unreacted starting material (Figure 3), which consists primarily of silica sol and brucite, at 0.02 and 0.035 Å^{-1}. There is a significant reduction of these humps after just 30 min of reaction time. For all samples from 1 to 48 h the curves are nearly identical (Figure 4). The feature at about 0.02 Å^{-1} remains throughout, albeit very weak,

(25) Muntean, J. V.; Stock, L. M.; Botto, R. E. *J. Magn. Reson.* **1988**, *76*, 540−542.

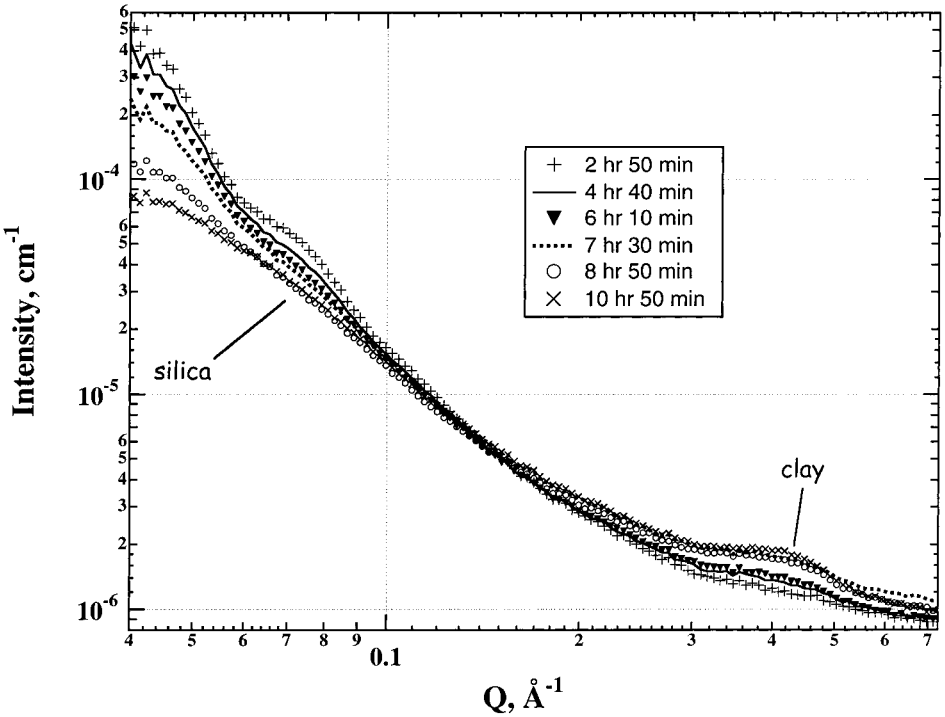

Figure 2. SAXS in the higher-*Q* data regime of in situ synthetic TEA−hectorite gel during crystallization at early stages. Only a few selected plots are shown for clarity as indicated in the legend. Silica agglomerates and the clay basal spacing are also indicated.

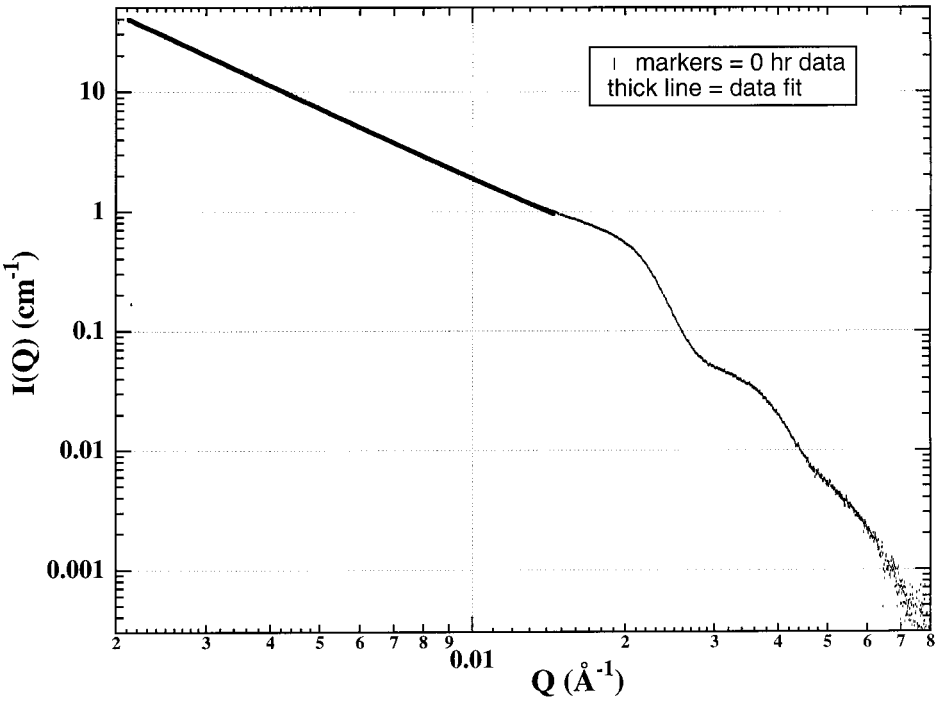

Figure 3. SAXS in the lower-*Q* data regime of the unreacted (0 h) synthetic TEA−hectorite powder sample. The power law data fit is shown with a slope of −1.99.

and is likely due to aggregation of particles. In fact, these curves can be fit using an extension of the unified equation developed by Beaucage[26] for multiple structural levels, with parameters inserted for a lamellar disk. This then in essence treats the system as aggregates of lamella. The data for the 0-h sample cannot be fit to this equation. This is to be expected because it is only a mixture of layered brucite and colloidal silica at this point. Instead, the scattering in the lowest-*Q* region can be fit to a simple power law equation with an exponent of −1.99 (indicated in Figure 3). This is measured as the negative slope of log(intensity) vs log(magnitude of the scattering vector, or *Q*) in a power law regime. A value of −2 occurs for disklike objects and is due to the layered brucite particles in this sample.[27]

(26) (a) Hyeon-Lee, J.; Beaucage, G.; Pratsinis, S. E.; Vemury, S. *Langmuir* **1998**, *14*, 5751. (b) Beaucage, G. *J. Appl. Crystallogr.* **1995**, *28*, 717.

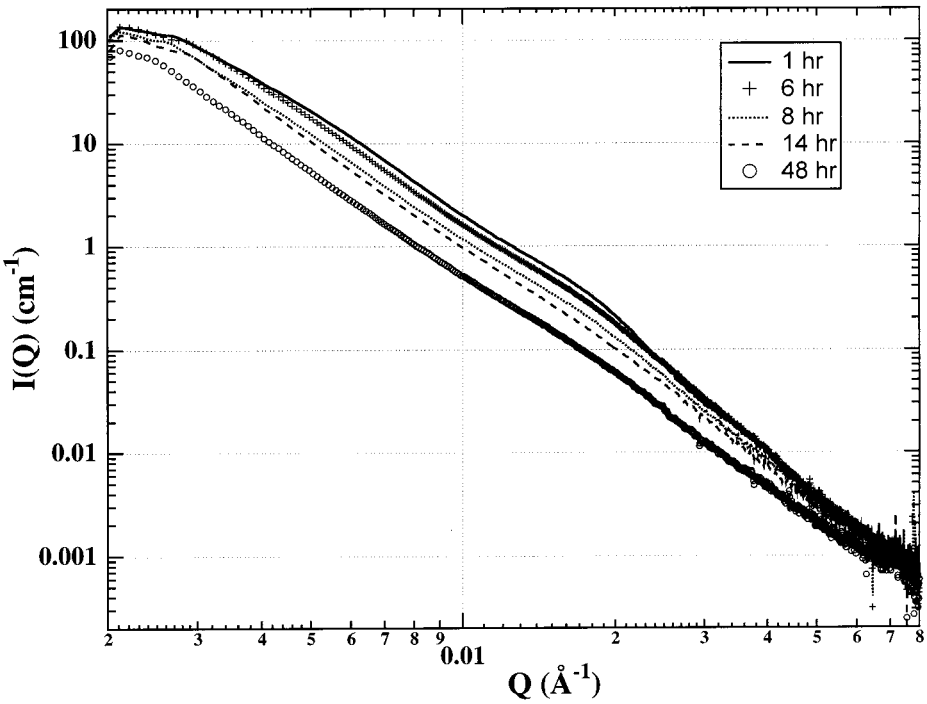

Figure 4. SAXS in the lower-*Q* data regime of the synthetic TEA−hectorite powder samples taken at various crystallization times.

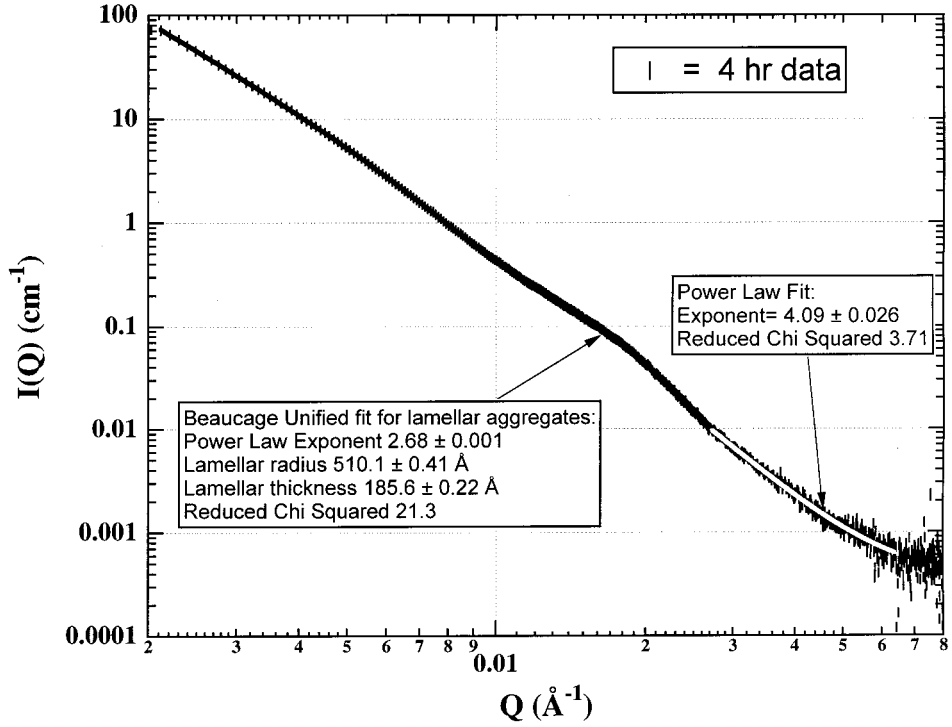

Figure 5. SAXS in the lower-*Q* data regime of the synthetic TEA−hectorite powder sample after 4 h of reaction. Two data fits are used as discussed in the text (dark line = Beaucage unified fit for lamellar aggregates; white line = power law fit with slope of −4.09).

A modified Guinier analysis of these data[3] yields a "thickness" of 33.5 Å, which reflects the not surprising fact that a few brucite layers are stacked in this powder.

Figure 5 shows the corrected scattering curve for the 4 h sample and includes the data fits as an example. The Beaucage unified fit works very well for these samples over the region of $0.0021 < Q < 0.03$ Å^{-1}. It does not correlate well at the higher *Q* values, however. Instead, here the curves fit to simple power laws with slopes of −4. This corresponds to Porod's law and reflects a large growth of the average particle radius.[27,28] The crossover between power laws occurs at values between 200 and 300 Å.

(27) Windsor, C. G. *J. Appl. Crystallogr.* **1988**, *21*, 528.

(28) Dokter, W. H.; van Garderen, H. F.; Beelen, T. P. M.; de Haan, J. W.; van de Ven, L. J. M.; van Santen, R. A. *Colloids Surf. A* **1993**, *72*, 165.

Table 1. Parameters from Unified Fits to Low-*Q* SAXS Data of Hectorite Powders

crystallization time (h)	Beaucage power law exponent	lamellar radius, Å	lamellar thickness, Å	high-*Q* power law exponent[a]
0.5	2.39	507	136	4.07
1	2.38	503	160	4.21
2	2.62	508	180	4.13
4	2.68	510	185	4.09
6	2.71	521	180	4.22
8	2.88	533	181	4.17
10	2.89	570	196	4.05
12	3.20	538	198	4.14
14	3.32	517	193	4.05
22	3.47	508	180	3.63
48	3.36	556	201	3.84

[a] Simple power law fit (not a Beaucage unified fit).

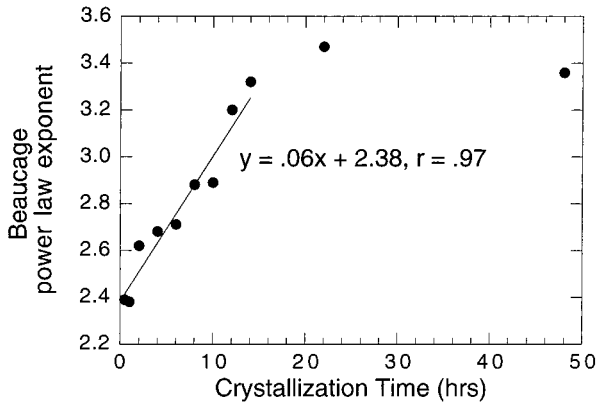

Figure 6. Plot of the power law exponents determined via the unified fit of Beaucage[26] (as shown in Figure 5 for an example) vs crystallization time of synthetic TEA−hectorite clay.

Table 1 lists the power law exponents, lamellar radii, and lamellar particle thicknesses from the fits for all of the powder aliquots. There is a steady progression in power law exponent up to the 14-h time frame as demonstrated in Figure 6. From earlier AFM data we proposed[5] that strands of brucite progress to particles of clay layers with tendrils of silica "glue" and that these further progress to more cemented aggregates of particles of clay layers. More specifically, the AFM data show that between 4 and 8 h nucleation of the clay crystallites is occurring and that at some point between 8 and 14 h the nucleation is complete. At times longer than 14 h, particles appeared to primarily coalesce and form substantially larger aggregates. We propose that the change in the low-*Q* SAXS power law also is reflecting the whole particle at early stages of clay nuclei with silica tendrils, which would be a more open structure, change to the more cemented, dense agglomerate at later times. The lamellar radii values in Table 1 do not change significantly with time. This is primarily because this particular parameter is dependent upon the point at which an "end" to the fit is chosen (at about $Q = 0.027$ Å^{-1}). The lamellar thicknesses, however, do increase somewhat with time. This increase is from 136 Å at 0.5 h to 201 Å at 48 h and corresponds to an increase of about 9 to 13 average stacked TEA−clay layers. This also explains the enhanced XRD signals observed with crystallization time.[4]

To be consistent, and for ease of sample preparation, only isolated and dried samples were compared by AFM and low-*Q* SAXS. As stated earlier, SAXS data from gels in this regime were not considered for further analysis because of the silica interference. This is not to say that we expect both powder and gel data to be the same in this regime because it is very likely that drying will induce discernible changes at these length scales as compared to the gels. Attempts to replace the silica sol with other (nonscattering) sources of silica have not thus far been successful.

Figure 7 is a SAXS plot where both low-*Q* and high-*Q* regimes for the 48-h powder sample are provided for demonstration purposes. Note the extended overlap that indicates good coverage of the entire *Q*-range (with no deviations at the limits of the SAXS cameras) and the fact that neither of these plots has been arbitrarily scaled in terms of their intensity.

NMR Studies. The ^{29}Si NMR data in Figure 8 displays a visible clay silicate peak at −94 ppm after just 1 h. This increases as the starting material Ludox silica peak at −112 ppm decreases, until the reaction is complete. The clay silicate peak at −94 ppm is readily assigned as the tetrahedral Q3(0Al) site reported previously at −94 to −95 ppm for natural hectorites.[13c,d,29] The term Q3 refers to the number of branching units typical of sheet silicate structures, and (0Al) indicates that no aluminum is present to effect the chemical shift. This assignment has been made also for the synthetic hectorite called Laponite at −94.4 ppm.[13c] The silica sol peak shifts from −112 to −109 ppm as the reaction proceeds and corresponds well to the published value: the Q4 tetrafunctional units of the silica sol (Ludox HS-40, while we used Ludox HS-30) are reported to occur at −107 ppm.[30] Some excess silica is present at the reaction's completion, which is not a surprise because it is also seen in XRD, SAXS, SANS, and chemical analyses[3] and has proven very difficult to remove.

There is an additional small peak in some of the ^{29}Si NMR plots at −85 ppm. This is due to a Q2 silica branching species that contains two hydroxyl groups, as has been observed in silica sols.[30] In the sols examined, the concentration of this Q2 peak at −85 ppm increased with decreasing particle size of the silica.[30] For the crystallizing TEA−hectorite samples, there is no evidence of the Q2 peak in the 0-h unreacted sample. As time goes on, a small feature at −85 ppm builds in up to a maximum at about 12 h of reaction. This would be expected if the initial Ludox silica sol particles were dissolving, becoming smaller, with the resultant species becoming more hydroxylated. This supports the view that small, dissolved silicate species (assumed to be tetrahedral) are condensing onto the pre-existing brucitic sheets.[3] Note that this peak is visible in the 4-h sample, the point at which a d(001) clay basal spacing is observed in XRD and SAXS. Note also that, at about the 12-h time frame, this component to the clay crystallization's mechanism of formation seems to be ending.

Tetraethylammonium (TEA) ions are used to aid crystallization and are incorporated as the exchange cations within the interlayers.[31] Figure 9 displays the

(29) Kinsey, R. A.; Kirkpatrick, R. J.; Hower, J.; Smith, K. A.; Oldfield, E. *Am. Miner.* **1985**, *70*, 537.

(30) Ramsay, J. D. F.; Swanton, S. W.; Matsumoto, A.; Goberdhan, D. G. C. In *The Colloid Chemistry of Silica*; Bergna, H. E., Ed.; Advances in Chemistry Series 234; American Chemical Society: Washington, DC, 1994; p 67.

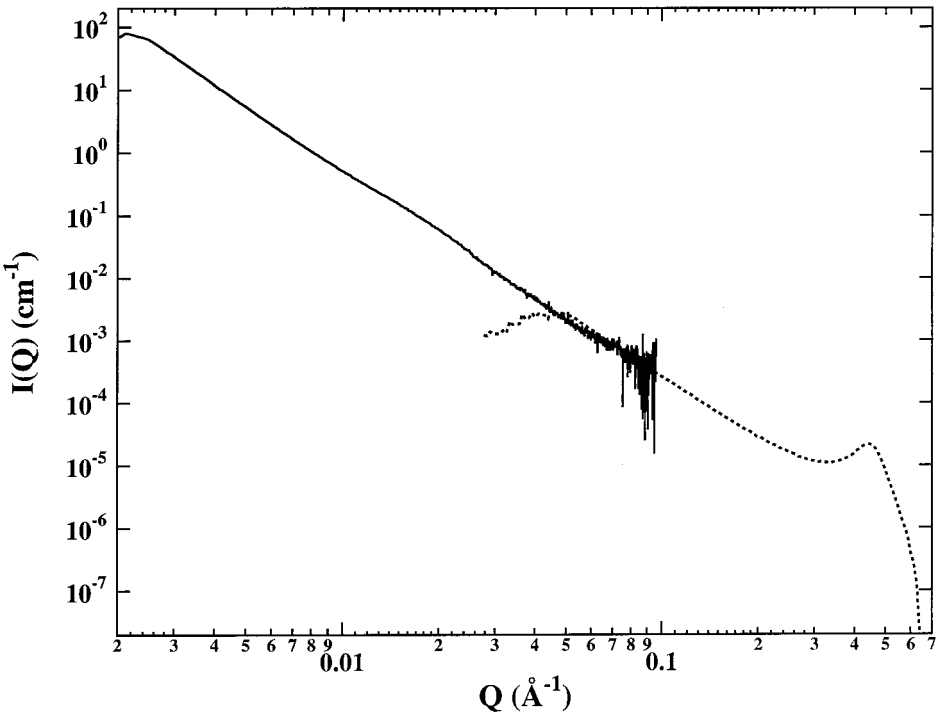

Figure 7. Combined SAXS plot of low-*Q* (solid line) and high-*Q* (dashed line) regimes of the data for the 48-h crystallized hectorite powder sample; no scaling of intensity was necessary.

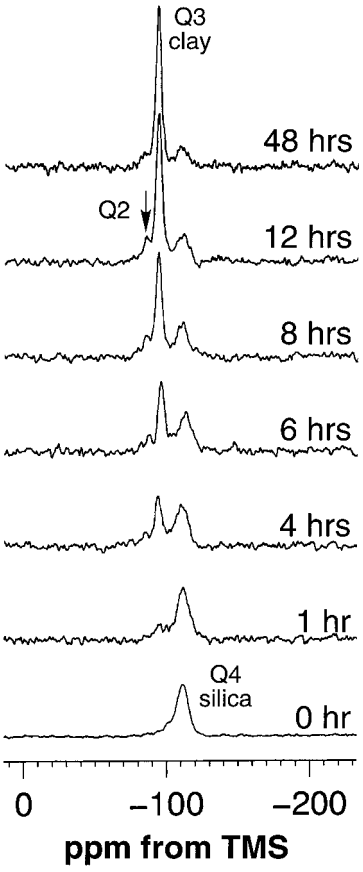

Figure 8. Solid-state ^{29}Si NMR for synthetic TEA−hectorite powders at increasing crystallization times.

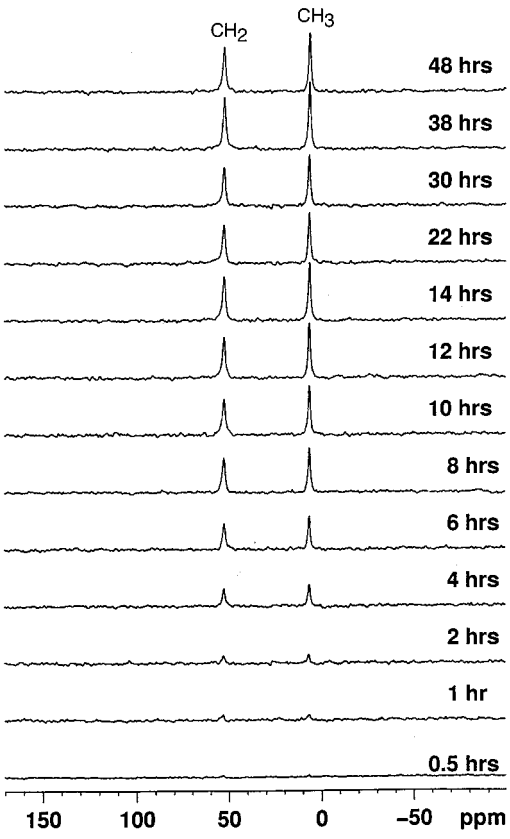

Figure 9. Solid-state ^{13}C MAS NMR of the CH_3- and $-CH_2-$ TEA peaks during crystallization of TEA−hectorite (ex situ powders).

^{13}C NMR plots of several powder aliquots showing the methyl and methylene peaks (at 7.5 and 52.5 ppm, respectively) of TEA clearly growing in with time. In fact, this technique is so sensitive that in as little as 30−60 min there is enough TEA incorporation to be visible in the product. A plot of the normalized signal (by weight) with reaction time shows that 80% of the final TEA loading is accomplished in the first 10 h (see

(31) Barrer, R. M.; Dicks, L. W. R. *J. Chem. Soc. A* **1967**, 1523.

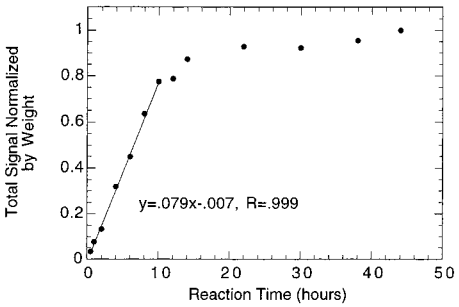

Figure 10. Correlation of TEA ^{13}C NMR signal intensity vs reaction time during the crystallization of TEA−hectorite.

Figure 10). After this the incorporation occurs at a much slower rate (in fact, about 20 times slower according to the slopes of the curve fits). Similar plots were obtained for the ^{29}Si NMR data (not shown), both for the loss of Q4 silica with time as well as the increase in Q3 clay signal. As with the SAXS power law data presented earlier, this is in agreement with AFM results[5] where Ostwald ripening is apparent in this system only in the early time frames.

Conclusions

The ex situ SAXS data, because they are in agreement with in situ data, confirm that vital information is not lost by isolating aliquots at various times for analysis by SAXS, at least in the high-*Q* regime. The NMR and low-*Q* SAXS data allow us to nearly pinpoint the time at which clay crystallites stop nucleating and begin to simply accrete and coalesce. Previous AFM studies had indicated that this occurred between 8 and 14 h for the hectorite system. After 10−12 h, ^{13}C NMR shows that 80% of the TEA has been incorporated in a linear fashion. The ^{29}Si NMR data also shows changes at this critical time in that a Q2 peak begins to fade, indicating that silica has perhaps stopped dissolving to a large extent. These clues may mean that just one mechanism is active during the early stages of nucleation and crystallization. Between 10 and 14 h there is a clear break in the NMR data of TEA uptake, after which AFM has shown that primarily agglomeration of particles is taking place. Power law values for the fits to the low-*Q* SAXS data indicate that this occurs in the 12−14-h time frame. Both AFM and SAXS indicate that structures are more "open" early on; AFM images reveal nuclei with several tendrils. With time these structures become more and more dense. The methods of SAXS, XRD, IR, and TGA are able to discriminate clay particles after about 4 h of reaction.[4] Solid-state ^{29}Si and ^{13}C NMR are more sensitive and able to pick up evidence of clay in as little as 30−60 min. Nearly all the techniques can distinguish a fairly radical change after about 14 h of reaction. At this time, peaks due to brucite disappear in XRD, AFM shows Ostwald ripening ending and accretion beginning, the rate of ^{13}C NMR signal intensity changes, and the rate in change of the SAXS power law also changes.

From all of these clues, it is proposed that the initial view of silica tetrahedra condensing to pre-existing brucitic sheets still holds.[3] Figure 11 shows a schematic of how we perceive this process proceeds with time. It is clear that, in a very short time (30−60 min), there is enough Li(I) incorporated for Mg(II) in the brucite sheet as well as enough silica tetrahedra condensed to that sheet, for the associated, charge-balancing TEA cation to be seen by ^{13}C NMR. Within 4 h, the sheets are larger and there are enough layer−layer correlations to allow detection of the d(001) peak by XRD and SAXS. As discussed in the preceding paragraph, there are numerous clues that after 14 h of reaction a change takes place. We propose that at this point the precursor pure brucite no longer exists. The remainder of the required 48-h crystallization time is needed to finalize Li(I) incorporation via occasional substitution of Mg(II), silicate condensation, and layer−layer correlations. This is provided by the small amounts of "nutrient gel" still associated with the particles as postulated from AFM images.[5] The particles also begin to coalesce after this time to ultimately 1−2 μm in size.

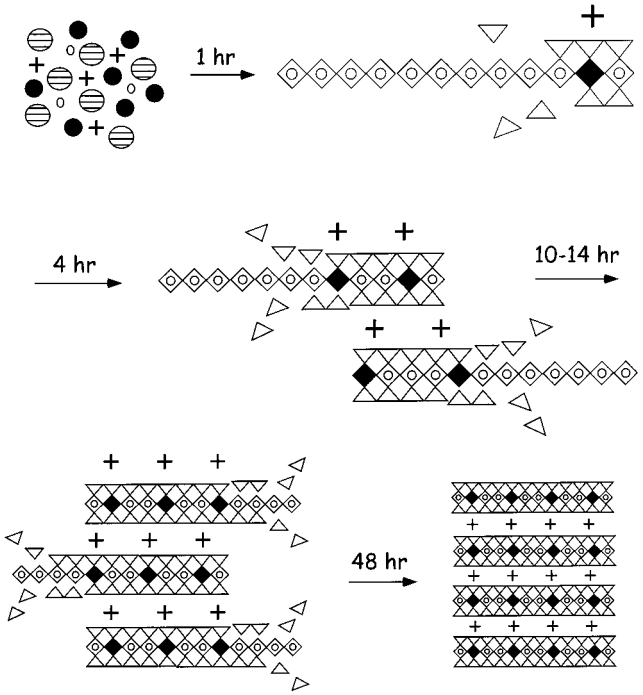

Figure 11. Possible schematic of a hectorite formation mechanism as inferred from the data collected here. A mixture of silica sol, brucite, LiF, and TEA (indicated as +) is heated for 1 h. At this point there is enough tetrahedral silicate (indicated by the triangles) coordination on the pre-existing brucitic sheets to be seen by ^{29}Si NMR as well as enough TEA association to be seen by ^{13}C NMR. The latter requires that some Li(I) be substituted for Mg(II) in the octahedral layer (indicated by the dark diamond). After 4 h, the clay sheets are large enough and there are enough layer−layer correlations to be seen by XRD and SAXS. After 10−14 h this process is nearly complete, but 48 h is required to optimize layer−layer correlations and TEA incorporation.

Acknowledgment. R. E. Winans, D. E. Alexander, M. Beno, and J. Linton of ANL are recognized for their help with various SAXS experimental details, as are K. Littrell (ANL) for devising the SAXS data analysis packages and P. Thiyagarajan and G. Sandí (ANL) for advising on the SAXS data analysis. J. Gregar of ANL sealed the SAXS sample cells for in situ heating. This research was performed under the auspices of the U.S. Department of Energy, Office of Basic Energy Sciences, Division of Chemical Sciences under Contract W-31-109-ENG-38 and benefited from the use of the APS at ANL.

CM000366A